Palladium Nanoparticles Supported on Ce-MOF-801 as Highly Efficient and Stable Heterogeneous Catalysts for Suzuki-Miyaura Coupling Reactions

Wenting Lin[1] · Yaping Song[1] · Li Wang[1] · Nan Li[1] · Yanghe Fu[1] · De-Li Chen[1] · Weidong Zhu[1] · Fumin Zhang[1]

Abstract

Palladium nanoparticles (Pd NPs) supported on a cerium-based metal–organic framework Ce-MOF-801 (Pd/Ce-MOF-801) was prepared using an incipient wetness impregnation strategy. Multiple analytical techniques were used to investigate the physicochemical properties of Pd/Ce-MOF-801. Afterwards, its catalytic efficiency in the Suzuki-Miyaura cross-coupling reaction between different haloarenes and phenylboronic acid was assessed. The developed Pd/Ce-MOF-801 displayed a high catalytic performance at 318 K and in the presence of K_2CO_3 as well as aqueous ethanol (as a solvent), much superior to Pd/Ce-BTC as well as the analogs reported in the literature by comprehensively comparing the catalytic activity and the relationship between reaction temperature and catalyst dosage. Moreover, the catalyst exhibited negligible Pd species leaching and was capable of being recycled in eight successive runs without any decay in reactivity. Such protocol has the advantages of ambient reaction conditions and tolerance to various substrates with various functional groups.

Graphical Abstract
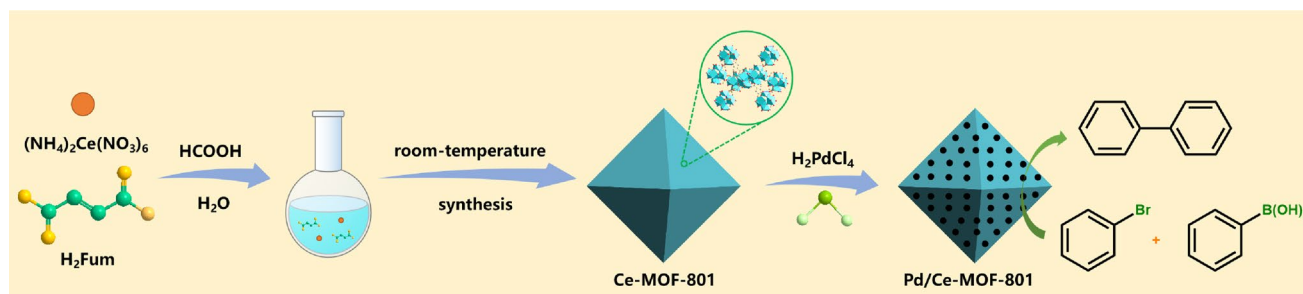
Keywords Catalysis · Nanocatalyst · Catalytic activity · C–C coupling reaction · Metal–organic framework

1 Introduction

Biaryl and its derivatives are widely used to produce polymers, pharmaceutical intermediates, bioactive compounds, and functional materials because of their unique and irreplaceable features [1–3]. Synthesis of these compounds via the carbon–carbon bond formation approach, such as the Suzuki-Miyaura coupling reaction catalyzed by Pd catalysts, is the central approach in modern synthetic chemistry [4–6]. Homogeneous catalysts, such as palladium complexes with nitrogen and phosphine-containing ligands, usually exhibited high catalytic activity and selectivity in this kind of transformation mainly due to the high intrinsic reactivity of Pd [7]. However, the expensive nature of palladium complexes along with issues regarding separation

✉ Fumin Zhang
zhangfumin@zjnu.edu.cn

[1] Key Laboratory of the Ministry of Education for Advanced Catalysis Materials, Institute of Physical Chemistry, Zhejiang Normal University, Jinhua 321004, People's Republic of China

and recyclability make it difficult to use these homogenous catalysts in practical applications.

To surmount these challenges and make the process fit the standards of green chemistry, researchers immobilized the palladium precursors on a range of porous materials, such as carbon [8–12], graphene [13–15], silica [16], zeolites [17], modified inorganic oxide [18], mesoporous materials [19, 20], and multi-walled carbon nanotube [21, 22], expecting to achieve stable, supported nanoparticles (Pd NPs) catalysts for the effective C–C bond forming reaction. Significantly, the particle size and dispersion of Pd NPs catalysts strongly influence their catalytic reactivity. The resilience of the recoverable and reusable materials against the leaching and agglomeration of the active sites is directly related to both of these properties at the same time [8, 9, 16]. Typically, a supporting substrate with a large specific surface area will yield supported Pd NPs catalysts. However, the resultant solid catalysts often displayed lower catalytic efficiency than the corresponding homogeneous analogs [20]. Even worse, the problems of leaching and aggregation of Pd NPs frequently occurred for some of these catalysts when used in liquid-phase media [21, 22]. Therefore, there is an urgent demand for highly active and stable supported Pd catalysts for the Suzuki-Miyaura coupling process.

Cerium oxide (CeO_2) is frequently utilized in heterogeneous catalysis [23], for example, in the oxidation of volatile organic compounds, partial hydrogenation, water–gas shift reaction, by virtue of their advantages of reversible Ce^{3+}/Ce^{4+} redox pairs, tailorable oxygen vacancies, and surface acid–base properties [24–26]. Moreover, recent studies have manifested that reducible CeO_2-supported Pd NPs presented a high catalytic activity in the Suzuki-Miyaura cross-coupling [26]. However, the deficiencies of CeO_2, such as low specific surface area and little availability of coordinate sites on the external surface, usually result in low loading and dispersion of metal NPs. Metal–organic frameworks (MOFs) have received considerable attention in heterogeneous catalysis owing to their large specific surface area, porous structure, and homogeneously distributed metal nodes [27–30]. MOFs are suitable for immobilizing metal NPs and other guest molecules with uniformly cage-like structures. Thus, various metal NPs@MOF composites were designed and tested in catalysis for several organic transformations, including coupling reactions [31–33], selective hydrogenation [34, 35], multi-component reactions [36], etc.

Ce-MOF-801, a cerium-based MOF with the molecular formula $Ce_6O_4(OH)_4(fumarate)_6$, is highly appropriate for immobilizing Pd NPs because of its large specific surface area abundant cage-like structure, as well as its high stability in a polar solvent (such as water) [37]. Moreover, approximately 10% of Ce^{3+} defect sites exist within this MOF's skeleton this means that at least one Ce^{3+} atom is present in about 50% of Ce_6 nodes [38]. These advantages

of Ce-MOF-801 may provide unique contributions to diverse catalytic redox processes, such as Suzuki-Miyaura cross-coupling. Therefore, this paper described a facile framework for making Pd/Ce-MOF-801 catalyst. Moreover, under benign circumstances, we effectively established its high catalytic activity and reusability in the Suzuki-Miyaura reaction. To our delight, the designed Pd/Ce-MOF-801 performs superior to that published in the literature.

2 Experimental

2.1 Catalyst Preparation
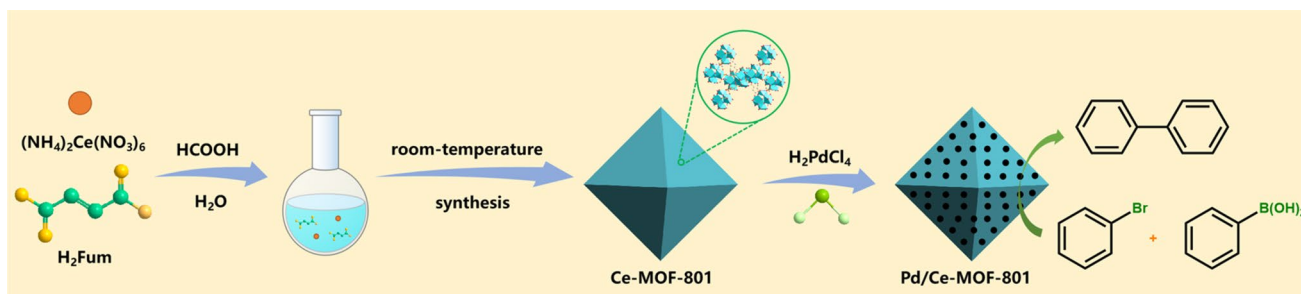
2.1.1 Synthesis of Ce-MOF-801

The Ce-MOF-801 nanocrystals were synthesized by a one-step room-temperature self-assembling approach [39]. A typical procedure began with the addition of 822 mg (1.5 mmol) of $(NH_4)_2Ce(NO_3)_6$ to a glass flask. Next, 2 mL of formic acid and 8 mL of distilled water were poured into the flask, and then the mixture was violently stirred for a period of 5 min. Thereafter, the solution received 175 mg (1.5 mmol) of fumaric acid by dropwise addition. Within 12 h, the solution became very hazy, pointing to Ce-MOF-801 formation. The solid product was obtained by centrifugation, washed three times with water and ethanol, and dried under vacuum for 12 h at 343 K.

2.1.2 Preparation of 1 wt% Pd/Ce-MOF-801

A typical incipient wetness impregnation approach was used to prepare a nominal 1 wt% Pd/Ce-MOF-801 sample [40]. Specifically, a calculated amount of Ce-MOF-801 (0.1 g) was mixed with an aqueous solution of H_2PdCl_4 (32.3 mg/mL, 31 μL) to obtain the impregnated sample. The wet sample was aged at 298 K for 24 h, followed by 12 h of vacuum oven drying at 373 K. To obtain the supported catalyst, the resulting solid was reduced with 20 mol% H_2 at 523 K for 4 h.

2.2 Suzuki-Miyaura Cross-Coupling Reaction

In a typical reaction, a solvent (4 mL) was combined with catalyst (4 mg, 0.1 mol% Pd), bromobenzene (0.32 mmol), phenylboronic acid (0.38 mmol), and base (0.38 mmol) in a Schlenk flask (10 mL in capacity), respectively (Scheme 1). Flask was hermetically sealed and heated to 318 K for the specified time. The reaction mixture was quantitatively analyzed by gas chromatography (Shimadzu, GC-2014) with InertCap five capillary column. The products were also confirmed by NMR spectroscopy. For the reusability evaluation, the spent Pd/Ce-MOF-801 catalyst was centrifuged, rinsed

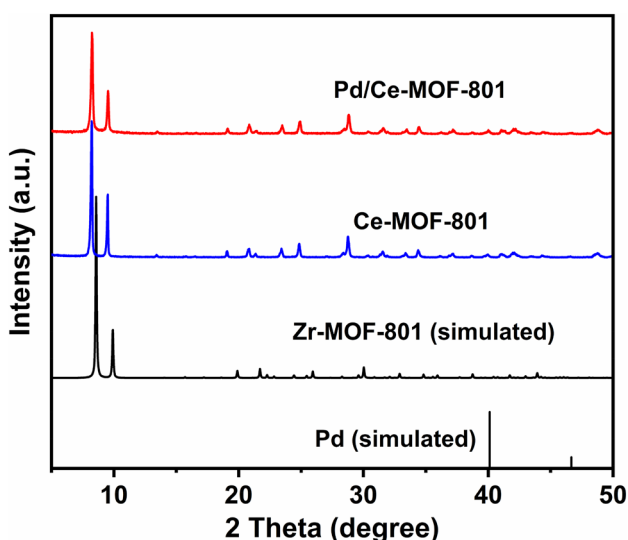**Scheme 1** A schematic illustration of the synthesis of Pd/Ce-MOF-801

Fig. 1 The powder XRD patterns of various samples

Fig. 2 The N_2 adsorption/desorption isotherms of Ce-MOF-801 and Pd/Ce-MOF-801

with ethyl acetate and water, heated at 393 K for 12 h, and reused without reduction.

3 Results and Discussion

3.1 Catalyst Characterization

The XRD patterns of the synthesized Ce-MOF-801 and Pd/Ce-MOF-801 are compared in Fig. 1. The simulated Zr-MOF-801 and the synthesized Ce-MOF-801 were nearly identical in terms of their line shape [39], without any diffraction peak associated with ceria appearing, implying that the as-prepared Ce-MOF-801 was a pure-phase MOF. For the Pd/Ce-MOF-801 catalyst, the skeleton network of Ce-MOF-801 was able to be well remained after the introduction of Pd precursor and further reduction treatment. However, due to the greater radii of Ce^{4+} (0.97 Å) compared to Zr^{4+} (0.84 Å), these reflections were also marginally pushed to lower 2θ values in Ce-MOF-801 and Pd/Ce-MOF-801.
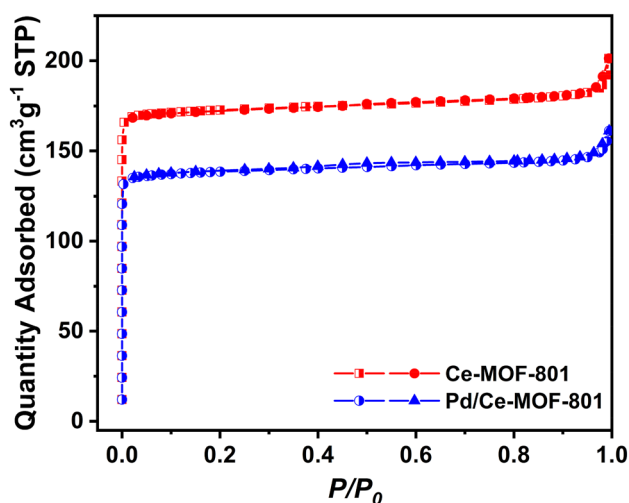
Additionally, similar to the pure Ce-MOF-801, Pd/Ce-MOF-801 did not exhibit any extra metal Pd-related Bragg peaks, which is likely due to the low Pd contents in the MOF. However, the intensities of the peaks were marginally reduced.

The N_2 adsorption/desorption isotherms of Ce-MOF-801 and Pd/Ce-MOF-801 are shown in Fig. 2. Both samples showed a sharp increase in adsorption at low relative pressures of $P/P_0 < 0.05$. Following the IUPAC nomenclature, the two samples displayed typical I-type isotherms, indicating the appearance of microporous structure in their frameworks [39]. Based on the nitrogen adsorption curves, the Brunauer–Emmett–Teller (BET) specific surface area and pore volume of Pd/Ce-MOF-801 were calculated to be 397.1 m^2/g and 0.25 cm^3/g, respectively. Both of these values were lower than those of pure Ce-MOF-801 (494.5 m2/g and 0.31 cm^3/g, respectively), indicating that Pd NPs were successfully immobilized within the MOF framework. The Fourier transform infrared (FTIR) spectra of Ce-MOF-801 and Pd/Ce-MOF-801 are shown in Fig. S1. Briefly, the

asymmetric (1550 cm^{-1}) and symmetric (1390 cm^{-1}) strong stretching vibrations of the carboxylate groups were present in the Pd/Ce-MOF-801 crystals [39]. Furthermore, the peak at 990 cm^{-1} was related to the stretching vibration peak of C=C, and 667 cm^{-1} was the symmetric vibration stretching peak of the Ce–O bond in the structure of Pd/Ce-MOF-801. These peaks were in close agreement with those of Ce-MOF-801 at similar positions. The TGA curve of Pd/Ce-MOF-801 revealed good thermal stability up to 573 K (Fig. S2).

The morphology was investigated by SEM analysis. Figure 3a showed the morphology of Ce-MOF-801, exhibiting a typical irregular shape and polyhedral structure. After immobilizing Pd NPs, there was no essential change in the morphology and porous structure for the prepared Pd/Ce-MOF-801 compared with Ce-MOF-801, but the color of the samples changed from faint yellow to grey. In the Pd/Ce-MOF-801 solid, the Pd NPs were highly dispersed (black dots) over the Ce-MOF-801 support without any significant aggregation (Fig. 3c). The Pd NPs with a mean size of 9 nm were estimated by calculating more than 200 randomly selected particles (Fig. 3d). The support Ce-MOF-801 showed gray color with lighter contrast due to their compositions of light elements (low Z value). The loading of metal Pd on Ce-MOF-801 was determined by inductively coupled plasma atomic emission spectroscopy (ICP-AES), and the results showed that the content of Pd was 1 wt%.

To determine the chemical oxidation state of Pd and Ce in Pd/Ce-MOF-801, X-ray photoelectron spectroscopy (XPS) measurements were performed. The high-resolution XPS spectra of Ce 3d acquired from Pd/Ce-MOF-801 are presented in Fig. 4a. The binding energy located at 904.0 eV,

885.6 eV, and 880.6 eV were belong to Ce^{3+} and the typical characteristic peaks at 906.6 eV, 900.6 eV, 888.0 eV, and 882.2 eV were assigned to Ce^{4+} [41]. The results indicated that the Ce^{3+}/Ce^{4+} couple co-existed in the Pd/Ce-MOF-801. The presence of Ce^{3+} suggests the loss of oxygen in Ce-MOF-801, which is related to the oxygen vacancies [42]. Moreover, the XPS of the fresh Pd/Ce-MOF-801 exhibited two strong binding energy peaks at 335.2 and 340.4 eV for the 3d 5/2 and 3d 3/2 core levels, respectively, indicating that the metallic palladium species in the catalyst (Fig. 4b) [43]. Additionally, a slight amount of the oxidized Pd species appeared in the sample, which may be due to the exposure of Pd/Ce-MOF-801 to air. High-resolution XPS spectra of O 1 s showed three distinct peaks, which correspond to lattice oxygen, surface active oxygen, and adsorbed oxygen, as shown in Fig. 4c [44]. In the Pd/Ce-MOF-801, the significant amount of oxygen vacancies is shown by the finding that the lattice oxygen content is low while the amount of surface-active oxygen is high [45]. We also verified the existence of oxygen vacancy by EPR spectroscopy (Fig. 4d). The result showed that Pd/Ce-MOF-801 had large oxygen vacancies and was likely beneficial for enhancing the catalytic behavior.

3.2 Catalytic Properties

Using the cross-coupling of bromobenzene and phenylboronic acid as a probe reaction, we started investigating the catalytic performance of Pd/Ce-MOF-801 in the Suzuki-Miyaura reaction after finishing the catalyst characterizations. When using 0.1 mol% (4 mg) palladium to bromobenzene, Pd/Ce-MOF-801 gave a biphenyl yield

Fig. 3 SEM images of **a** Ce-MOF-801 and **b** Pd/Ce-MOF-801; TEM image **c** and **d** the corresponding particle size distribution pattern of Pd/Ce-MOF-801
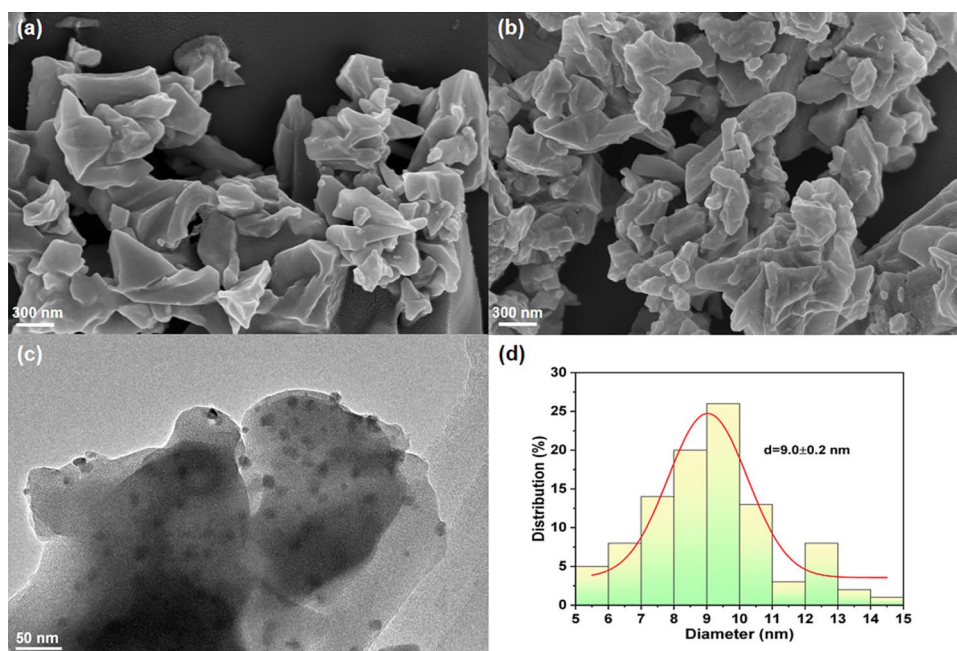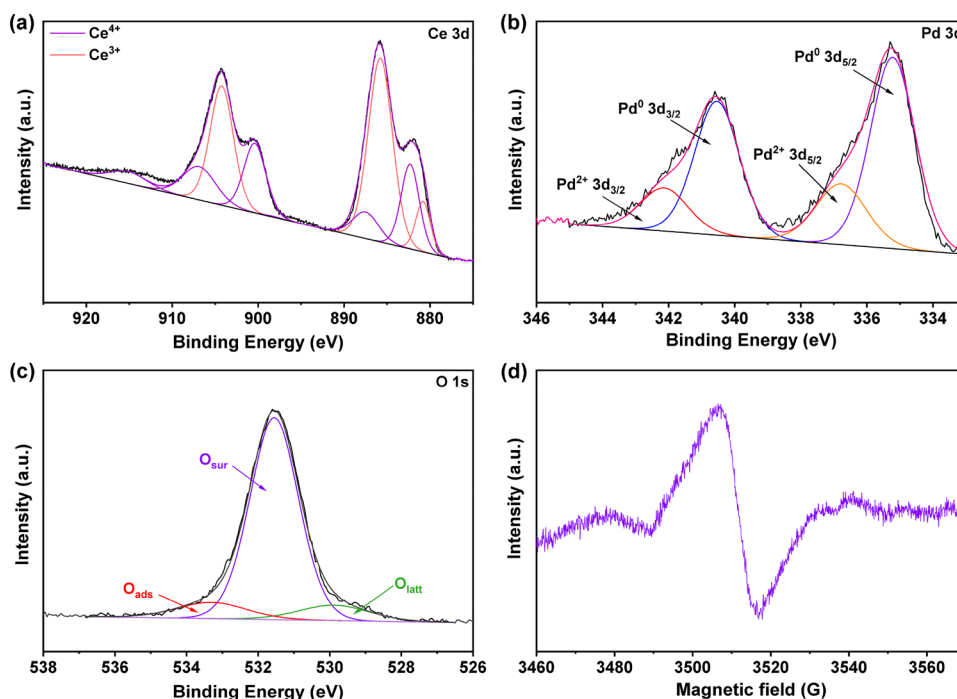
of 94.5% after reacting at 318 K for a short time of 0.5 h (entry 6, Table 1). Notably, the target product biaryl was obtained with a 100% selectivity. However, only a limited product was generated over the parent MOF supports (entry 1), implying that the active Pd site was intrinsically indispensable for this kind of coupling reaction. Moreover, a control catalyst, Pd/Ce-BTC, was also prepared and evaluated (Figs. S3–S7 in SI), e.g., Pd NPs supported on Ce-BTC, achieved only a 16.6% yield (entry 3), likely owing to its low specific surface and pore volume.

The influence of other bases on the probe reaction was investigated, including K_2CO_3, $NaHCO_3$, Et_3N, NaOH, Cs_2CO_3, and Na_2CO_3. Comparing K_2CO_3 to different organic and inorganic bases, as indicated in Table 1, it was observed that K_2CO_3 is a suitable base to supply the desired product with the best yield and relatively quick reaction time (entry 6, Table 1). Moreover, the amount of K_2CO_3 usage was also optimized, and the optimal dosage was 0.38 mmol. Additionally, a considerable solvent effect was seen after more solvent screening. Notable, in the presence of Pd/Ce-MOF-801, aqueous EtOH (v/v, 1:1) gave the maximum yield in the shortest time (0.5 h). While in other solvents such as H_2O, aqueous acetonitrile, and DMF, lower results were observed (entries 14–22, Table 1). Based on the intended product yield, 50% EtOH was ultimately the best-suited solvent for the probe reaction. From Table S1, it was noticed that the transformation did not outcome satisfactory yields at different temperatures like 313 K (entry 3, Table S2), and the optimum result was obtained at 318 K.

To ascertain the reaction's kinetic characteristics, bromobenzene and phenylboronic acid were coupled over Pd/Ce-MOF-801. This was done at various temperatures. It was anticipated that the coupling rate wouldn't depend on the amount of phenylboronic acid present (fivefold to bromobenzene) [46]. As can be seen in Fig. 5a, the pseudo-first-order kinetics provided a good match for the couplings at the three different temperatures, and rate constants (*k*) could be calculated as the inverse of the slope of the curve. The activation energy (E_a) for the Suzuki-Miyaura coupling system over Pd/Ce-MOF-801 was then calculated to be 74.8 kJ/mol (Fig. 5b), which is quite similar to that mediated by other Pd-based catalysts reported in the literature [46].

Subsequently, we studied the effect of the removal of Pd/Ce-MOF-801 on the cross-coupling of bromobenzene and phenylboronic acid (the hot filtration test). The supported Pd-based catalyst was isolated from the liquid mixture upon reacting for 10 min, and the coupling reaction was allowed to continue for an additional 20 min. During this period, no further increase in the product yield was measured upon catalyst removal (Fig. 5c). The amount of Pd leaching in the reaction medium was analyzed by ICP-AES analysis, which confirmed that only a negligible amount of Pd was leached during the coupling reaction. However, due to the complexity of the cross-coupling reaction, further in-depth experiment work is still needed to demonstrate whether its mechanistic nature is homogeneous or heterogeneous catalysis.

Furthermore, the Pd/Ce-MOF-801 could be easily and successfully separated from the reaction mixture after coupling. It could then be rinsed appropriately with aqueous

Table 1 Optimization of the reaction conditions of the Suzuki-Miyaura cross-coupling

Entry	Base	Alkali dosage (mmol)	Solvent	Time (h)	Yield (%)
1[a]	K_2CO_3	0.38	Ethanol/H_2O	4	3.1
2[b]	K_2CO_3	0.38	Ethanol/H_2O	4	6.6
3[c]	K_2CO_3	0.38	Ethanol/H_2O	0.5	16.6
4	$NaHCO_3$	0.38	Ethanol/H_2O	2	44.2
5	Na_2CO_3	0.38	Ethanol/H_2O	0.5	90.1
6	K_2CO_3	0.38	Ethanol/H_2O	0.5	94.5
7	Cs_2CO_3	0.38	Ethanol/H_2O	0.5	85.2
8	NaOH	0.38	Ethanol/H_2O	2	66.5
9	Et_3N	0.38	Ethanol/H_2O	2	25.0
10	K_2CO_3	0.16	Ethanol/H_2O	0.5	54.5
11	K_2CO_3	0.32	Ethanol/H_2O	0.5	87.6
12	K_2CO_3	0.64	Ethanol/H_2O	0.5	84.7
13	K_2CO_3	0.96	Ethanol/H_2O	0.5	85.2
14	K_2CO_3	0.38	Ethanol	2	5.8
15	K_2CO_3	0.38	DMF/H_2O[d]	0.5	30.6
16	K_2CO_3	0.38	DMF	2	18.6
17	K_2CO_3	0.38	Acetone/H_2O[e]	0.5	91.2
18	K_2CO_3	0.38	Acetone	2	3.3
19	K_2CO_3	0.38	Acetonitrile/H_2O[f]	2	6.0
20	K_2CO_3	0.38	Acetonitrile	2	1.8
21	K_2CO_3	0.38	Toluene	2	2.9
22	K_2CO_3	0.38	H_2O	2	16.5

Reaction conditions: A mixture of 0.32 mmol of bromobenzene, 0.38 mmol of phenylboronic acid, 4 mg (0.1 mol%) of Pd/Ce-MOF-801, and 4 mL of solvent (Ethanol/H_2O = 1:1) at 318 K

[a]Ce-MOF-801 (4 mg)

[b]Ce-BTC (4 mg)

[c]Pd/Ce-BTC (0.1 mol%)

[d]DMF/H_2O = 1:1

[e]Acetone/H_2O = 1:1

[f]Acetonitrile/H_2O = 1:1

EtOH before being put through the next run without additional reduction treatment. The Pd/Ce-MOF-801 nanocomposite displayed stable catalytic behavior up to eight successive cycles without any decay in reactivity (Fig. 5d). We further analyzed the crystal structure, porous property, and Pd dispersion of the used Pd/Ce-MOF-801 catalyst after recycling 8 times using XRD, N_2 adsorption isotherm, and TEM (Figs. S8–S10). The results showed that the spent catalyst retains its initial crystal structure without any change in the Pd NPs size, which in turn validates the robustness of the Ce-MOF-801-stabilized Pd NPs catalyst.

Based on the literature and our experimental results, the cross-coupling reaction mechanism is tentatively deduced [26, 47, 48]. Ce^{3+} cations and the O vacancy were formed during the synthesis process of Ce-MOF-801. In the initial stage of the Suzuki-Miyaura coupling, the active $OH^{\delta-}$ groups were likely in situ created via the adsorption and dissociation of H_2O on the O-vacancy sites. Subsequently, the electrons transfer to the Pd NPs was significantly promoted on account of the electron-donating effect between the Ce^{3+} cations and $OH^{\delta-}$ (as the electron pair donors), which positively impacted the oxidative addition of aryl halide. This step was regarded as the rate-determining step in the C–C coupling reactions to form the critical intermediate $ArPd^{II}X$, and it subsequently promoted the catalytic activity of Pd for the C–C coupling reactions.

Additionally, Pd/Ce-MOF-801 was used to couple a variety of haloarenes with phenylboronic acid in the most favorable reaction circumstances to research the substrate range and functional group tolerance (Table 2). The catalytic systems described here were capable of withstanding a variety of functional groups under the conditions of the current reaction (entries 1–12, Table 2). Excitingly, Pd/Ce-MOF-801 efficiently boosted the Suzuki-Miyaura coupling of these aryl halides with phenylboronic acid to the desired biphenyl compounds with excellent efficiency. Aryl halides substrates with electron-withdrawing, and electron-donating substituents, including methyl, formyl, methoxyl, nitro, and ester groups, yielded the corresponding products selectively and efficiently. Overall, these results suggest a broad range of substrates and functional groups were well tolerated by our Pd/Ce-MOF-801 catalyst. Moreover, all NMR spectra were in agreement with those described in the literature [49–51], supporting the effective synthesis of the targeted compounds.

In order to demonstrate the superiority of the catalytic system we developed, a thorough comparison with other widely used methods for coupling bromobenzene and phenylboronic acid has been conducted. The Pd/Ce-MOF-801 nanocomposite revealed a superior activity by comprehensively comparing reaction conditions and the product yield (Table S3).
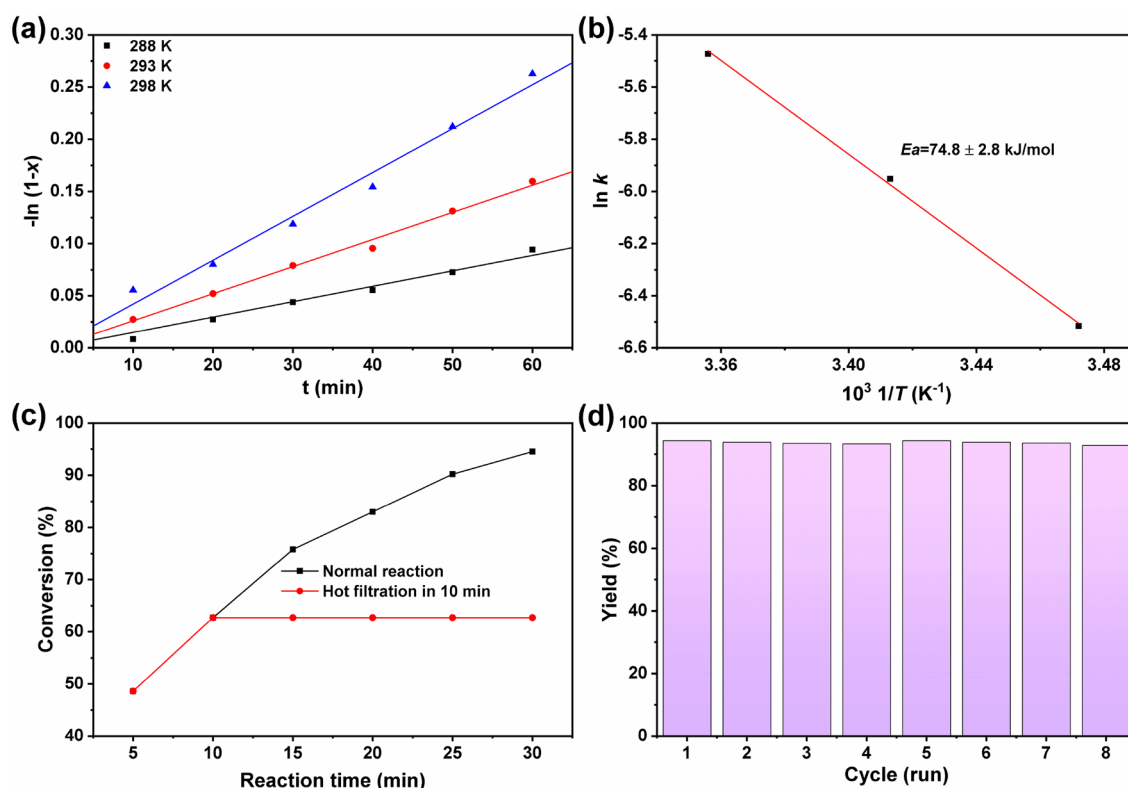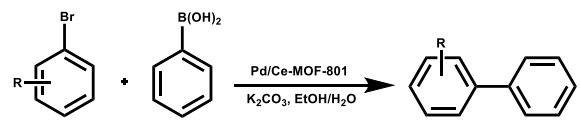
Fig. 5 **a, b** Kinetic studies of the Suzuki-Miyaura cross-coupling of bromobenzene and phenylboronic acid over Pd/Ce-MOF-801; **c** Effect of the removal of Pd/Ce-MOF-801 during the reaction; **d** Recycling r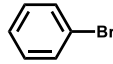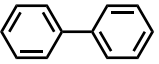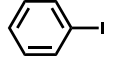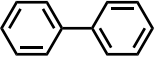esults. *Reaction conditions* 0.32 mmol of bromobenzene, 0.38 mmol of phenylboronic acid, and 0.38 mmol of K_2CO_3 in 4 ml of Ethanol/H_2O (v/v, 1:1) mixed solvents by using 4 mg of Pd/Ce-MOF-801 (0.1 mol% Pd), 318 K, 0.5 h
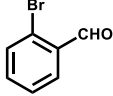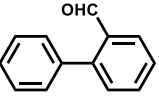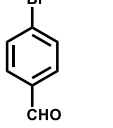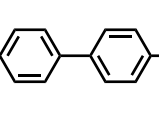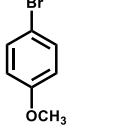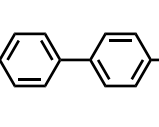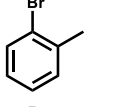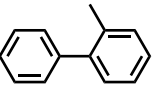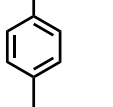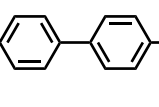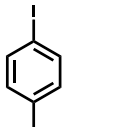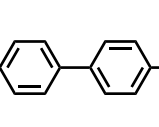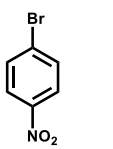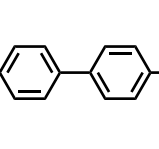
4 Conclusions

Ce-based MOF Ce-MOF-801 nanocrystals were synthesized by a facile one-step room-temperature synthesis method, then Pd NPs loaded on Ce-MOF-801 solids was successfully prepared by an incipient wetness impregnation technique. The synthesized Pd/Ce-MOF-801 catalyst acted as a highly effective heterogeneous catalyst for Suzuki-Miyaura cross-coupling reactions under mild reaction conditions, with markedly improved activity compared to Pd/Ce-BTC as well as analogs described in the literature. The excellent catalytic performance of the developed Pd/Ce-MOF-801 is likely related to the large specif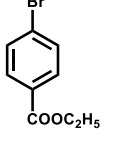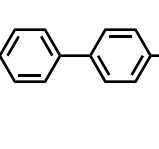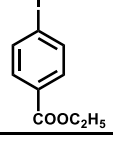ic surface area, highly dispersed Pd NPs, and an appropriate number of Ce^{3+} defect sites within the catalyst. Advantages of our strategy include efficient heterogeneous catalysis at relatively mild conditions, less usage of rare palladium metal, a shorter reaction time, and easy catalyst recycling and reuse, as compared to traditional homogeneous approaches. However, inexpensive and large-scale synthesis of Ce-MOF-801 is still one of the prerequisites for its practical application.

Table 2 Substrate scope of the Suzuki-Miyaura cross-coupling over Pd/Ce-MOF-801

Entry	Aryl halide	Products	Yield (%)
1			94.5
2			95.7
3			95.8
4[b]			95.1
5			90.4
6			94.5
7			97.3
8			98.5
9			>99
10			>99
11			>99

Table 2 (continued)
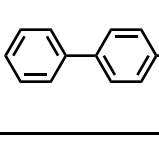
Reaction conditions: 0.32 mmol of aryl halide, 0.38 mmol of phenylboronic acid, and 0.38 mmol of K_2CO_3 in 4 ml of Ethanol/H_2O (v/v, 1:1) mixed solvents by using 4 mg of Pd/Ce-MOF-801 (0.1 mol% Pd), 318 K, 0.5 h. [b]353 K, 2 h

Supplementary Information The online version contains supplementary material available at https://doi.org/10.1007/s10562-022-04163-4.

Author Contributions WL: investigation, methodology, writing—original draft. YS: methodology. LW: methodology. NL: methodology. YF: writing—original draft. De-LiC: writing—original draft. WZ: project administration. FZ: conceptualization, project administration, supervision, Writing—review & editing.

Declarations

References

1. Wang J, Liu CF, Zheng Q et al (2020) C-H functionalization of biaryl compounds. Eur J Org Chem 2020:3737–3765
2. Jain ZJ, Gide PS, Kankate RS (2017) Biphenyls and their derivatives as synthetically and pharmacologically important aromatic structural moieties. Arab J Chem 10:S2051–S2066
3. Felpin FX, Sengupta S (2019) Biaryl synthesis with arenediazonium salts: cross-coupling, CH-arylation and annulation reactions. Chem Soc Rev 48:1150–1193
4. Wu XF, Anbarasan P, Neumann H et al (2010) From noble metal to nobel prize: palladium-catalyzed coupling reactions as key methods in organic synthesis. Angew Chem Int Ed 49:9047–9050
5. Balanta A, Godard C, Claver C (2011) Pd nanoparticles for C-C coupling reactions. Chem Soc Rev 40:4973–4985
6. Maluenda I, Navarro O (2015) Recent developments in the Suzuki-Miyaura reaction: 2010–2014. Molecules 20:7528–7557
7. Das P, Linert W (2016) Schiff base-derived homogeneous and heterogeneous palladium catalysts for the Suzuki-Miyaura reaction. Coord Chem Rev 311:1–23
8. Bugday N, Altin S, Yasar S (2021) Palladium nanoparticle supported on nitrogen-doped porous carbon: investigation of structural properties and catalytic activity on Suzuki-Miyaura reactions. Appl Organomet Chem 35:1–23
9. Veerabagu U, Chen ZB, Xiang J et al (2021) Novel cigarette butts-derived porous carbon-based catalyst for highly efficient Suzuki-Miyaura cross-coupling reaction. J Environ Chem Eng 9:1–10
10. Zhang L, Feng C, Gao ST et al (2015) Palladium nanoparticle supported on metal-organic framework derived N-decorated nanoporous carbon as an efficient catalyst for the Suzuki coupling reaction. Catal Commun 61:21–25
11. Dong WH, Zhang L, Wang CH et al (2016) Palladium nanoparticles embedded in metal-organic framework derived porous carbon: synthesis and application for efficient Suzuki-Miyaura coupling reactions. RSC Adv 6:37118–37123

12. Zhang L, Dong WH, Shang NZ et al (2016) N-Doped porous carbon supported palladium nanoparticles as a highly efficient and recyclable catalyst for the Suzuki coupling reaction. Chin Chem Lett 27:149–154

13. Shang NZ, Feng C, Zhang HY et al (2013) Suzuki-Miyaura reaction catalyzed by graphene oxide supported palladium nanoparticles. Catal Commun 40:111–115

14. Shang NZ, Gao ST, Feng C et al (2013) Graphene oxide supported N-heterocyclic carbene-palladium as a novel catalyst for the Suzuki-Miyaura reaction. RSC Adv 3:21863–21868

15. Gao ST, Shang NZ, Feng C et al (2014) Graphene oxide-palladium modified Ag-AgBr: a visible-light-responsive photocatalyst for the Suzuki coupling reaction. RSC Adv 4:39242–39247

16. Polshettiwar V, Len C, Fihri A (2009) Silica-supported palladium: sustainable catalysts for cross-coupling reactions. Coord Chem Rev 253:2599–2626

17. Durap F, Rakap M, Aydemir M et al (2010) Room temperature aerobic Suzuki cross-coupling reactions in DMF/water mixture using zeolite confined palladium (0) nanoclusters as efficient and recyclable catalyst. Appl Catal A 382:339–344

18. Bankar DB, Hawaldar RR, Arbuj SS et al (2020) Palladium loaded on ZnO nanoparticles: synthesis, characterization and application as heterogeneous catalyst for Suzuki-Miyaura cross-coupling reactions under ambient and ligand-free conditions. Mater Chem Phys 243:1–10

19. Akkoc M, Bugday N, Altin S et al (2022) Highly active Fe_3O_4@SBA-15@NHC-Pd catalyst for Suzuki-Miyaura cross-coupling reaction. Catal Lett 152:1621–1638

20. Ziarani GM, Rohani S, Ziarati A et al (2018) Applications of SBA-15 supported Pd metal catalysts as nanoreactors in C-C coupling reactions. RSC Adv 8:41048–41100

21. Sargin I, Baran T, Arslan G (2020) Environmental remediation by chitosan-carbon nanotube supported palladium nanoparticles: conversion of toxic nitroarenes into aromatic amines, degradation of dye pollutants and green synthesis of biaryls. Sep Purif Technol 247:1–10

22. Sadjadi S, Heravi MM, Raja M (2018) Combination of carbon nanotube and cyclodextrin nanosponge chemistry to develop a heterogeneous Pd-based catalyst for ligand and copper free C-C coupling reactions. Carbohyd Polym 185:48–55

23. Montini T, Melchionna M, Monai M et al (2016) Fundamentals and catalytic applications of CeO_2-based materials. Chem Rev 116:5987–6041

24. Chen XD, Su X, Liang BL et al (2016) Identification of relevant active sites and a mechanism study for reverse water gas shift reaction over Pt/CeO_2 catalysts. J Energy Chem 25:1051–1057

25. Wang PF, Wang J, Shi J et al (2020) Low content of samarium doped CeO_2 oxide catalysts derived from metal organic framework precursor for toluene oxidation. Mol Catal 492:1–10

26. Zhang S, Li J, Gao W et al (2015) Insights into the effects of surface properties of oxides on the catalytic activity of Pd for C-C coupling reactions. Nanoscale 7:3016–3021

27. Yang QH, Xu Q, Jiang HL (2017) Metal-organic frameworks meet metal nanoparticles: synergistic effect for enhanced catalysis. Chem Soc Rev 46:4774–4808

28. Evans JD, Garai B, Reinsch H et al (2019) Metal-organic frameworks in Germany: from synthesis to function. Coord Chem Rev 380:378–418

29. Razavi SAA, Morsali A (2019) Linker functionalized metal-organic frameworks. Coord Chem Rev 399:213023–213079

30. Kargar PG, Aryanejad S, Bagherzade G (2020) Simple synthesis of the novel Cu-MOF catalysts for the selective alcohol oxidation and the oxidative cross-coupling of amines and alcohols. Appl Organomet Chem 34:1–12

31. Carson F, Pascanu V, Gomez AB et al (2015) Influence of the base on Pd@MIL-101-NH$_2$ (Cr) as catalyst for the Suzuki-Miyaura cross-coupling reaction. Chem Eur J 21:10896–10902

32. Veisi H, Abrifam M, Kamangar SA et al (2021) Pd immobilization biguanidine modified Zr-UiO-66 MOF as a reusable heterogeneous catalyst in Suzuki-Miyaura coupling. Sci Rep 11:1–14

33. Dong DP, Li ZH, Liu DD et al (2018) Postsynthetic modification of single Pd sites into uncoordinated polypyridine groups of a MOF as the highly efficient catalyst for Heck and Suzuki reactions. New J Chem 42:9317–9323

34. Wang BQ, Liu WX, Zhang WN et al (2017) Nanoparticles@nanoscale metal-organic framework composites as highly efficient heterogeneous catalysts for size- and shape-selective reactions. Nano Res 10:3826–3835

35. Zhang WL, Shi WX, Ji WL et al (2020) Microenvironment of MOF channel coordination with Pt NPs for selective hydrogenation of unsaturated aldehydes. ACS Catal 10:5805–5813

36. Treesa GSS, Saranya S, Meera G et al (2020) Recent advances and perspectives in the silver-catalyzed multi-component reactions. Curr Org Chem 24:291–313

37. Lammert M, Wharmby MT, Smolders S et al (2015) Cerium-based metal organic frameworks with UiO-66 architecture: synthesis, properties and redox catalytic activity. Chem Commun 51:12578–12581

38. Rojas-Buzo S, Concepcion P, Olloqui-Sariego JL et al (2021) Metalloenzyme-inspired Ce-MOF catalyst for oxidative halogenation reactions. ACS Appl Mater Interfaces 13:31021–31030

39. Dai S, Nouar F, Zhang SJ et al (2021) One-step room-temperature synthesis of metal (IV) carboxylate metal-organic frameworks. Angew Chem Int Ed 60:4282–4288

40. Eskandari S, Tate G, Leaphart NR et al (2018) Nanoparticle synthesis via electrostatic adsorption using incipient wetness impregnation. ACS Catal 8:10383–10391

41. Zhang HF, Qiu JJ, Yan BC et al (2021) Regulation of Ce (III)/Ce (IV) ratio of cerium oxide for antibacterial application. iScience 24:1–23

42. Dutta P, Pal S, Seehra M et al (2006) Concentration of Ce^{3+} and oxygen vacancies in cerium oxide nanoparticles. Chem Mater 18:5144–5146

43. Kar AK, Kaur SP, Kumar TJD et al (2020) Efficient hydrogenolysis of aryl ethers over Ce-MOF supported Pd NPs under mild conditions: mechanistic insight using density functional theoretical calculations. Catal Sci Technol 10:6892–6901

44. Sun WJ, Li XM, Sun C et al (2019) Insights into the pyrolysis processes of Ce-MOFs for preparing highly active catalysts of toluene combustion. Catalysts 9:1–15

45. Zhang Q, Zhao XR, Duan LB et al (2020) Controlling oxygen vacancies and enhanced visible light photocatalysis of CeO_2/ZnO nanocomposites. J Photoch Photobiol A 392:1–10

46. Erunal E (2021) Estimation of the number of active sites through kinetic analysis on MWCNT-supported nanocatalysts. Int J Chem Kinet 53:954–963

47. Wang YG, Mei DH, Li J et al (2013) DFT+U study on the localized electronic states and their potential role during H_2O dissociation and CO oxidation processes on CeO_2 (111) surface. J Phys Chem C 117:23082–23089

48. Li YL, Zhang ZQ, Fan T et al (2016) Magnetic core-shell to yolk-shell structures in palladium-catalyzed Suzuki-Miyaura reactions: heterogeneous versus homogeneous nature. ChemPlusChem 81:564–573

49. Wang ZJ, Lv JJ, Feng JJ et al (2015) Enhanced catalytic performance of Pd-Pt nanodendrites for ligand-free Suzuki cross-coupling reactions. RSC Adv 5:28467–28473

50. Srimani D, Sawoo S, Sarkar A (2007) Convenient synthesis of palladium nanoparticles and catalysis of Hiyama coupling reaction in water. Org Lett 9:3639–3642

51. Ueura K, Satoh T, Miura M (2005) Rhodium-catalyzed arylation using arylboron compounds: efficient coupling with aryl halides and unexpected multiple arylation of benzonitrile. Org Lett 7:2229–2231